HHS Public Access

Author manuscript

Exp Eye Res. Author manuscript; available in PMC 2023 January 01.

Published in final edited form as:

Exp Eye Res. 2022 January ; 214: 108882. doi:10.1016/j.exer.2021.108882.

Histology and clinical imaging lifecycle of black pigment in fibrosis secondary to neovascular age-related macular degeneration

Ling Chen[a,b,1], **Dongfeng Cao**[b,1], **Jeffrey D. Messinger**[b], **Thomas Ach**[c], **Daniela Ferrara**[d], **K. Bailey Freund**[e,f], **Christine A. Curcio**[b,*]

[a]The First Affiliated Hospital of Chongqing Medical University, Chongqing Key Laboratory of Ophthalmology, Chongqing Eye Institute, Chongqing Branch of National Clinical Research Center for Ocular Diseases, Chongqing, PR China

[b]Department of Ophthalmology and Visual Sciences, University of Alabama at Birmingham School of Medicine, Birmingham, AL, USA

[c]Department of Ophthalmology, University Hospital Bonn, Bonn, Germany

[d]Genentech, South San Francisco, CA, USA

[e]Vitreous Retina Macula Consultants of New York, New York, NY, USA

[f]Department of Ophthalmology, New York University Grossman School of Medicine, New York, NY, USA

Abstract

Purpose: Melanotic cells with large spherical melanosomes, thought to originate from retinal pigment epithelium (RPE), are found in eyes with neovascular age-related macular degeneration (nvAMD). To generate hypotheses about RPE participation in fibrosis, we correlate histology to clinical imaging in an eye with prominent black pigment in fibrotic scar secondary to nvAMD.

Methods: Macular findings in a white woman with untreated inactive subretinal fibrosis due to nvAMD in her right eye were documented over 9 years with color fundus photography (CFP), fundus autofluorescence (FAF) imaging, and optical coherence tomography (OCT). After death (age 90 years), this index eye was prepared for light and electron microscopy to analyze 7 discrete zones of pigmentation in the fibrotic scar. In additional donor eyes with nvAMD, we determined the frequency of black pigment (n = 36 eyes) and immuno-labeled for retinoid, immunologic, and microglial markers (RPE65, CD68, Iba1, TMEM119; n = 3 eyes).

Results: During follow-up of the index eye, black pigment appeared and expanded within a hypoautofluorescent fibrotic scar. The blackest areas correlated to melanotic cells (containing large spherical melanosomes), some in multiple layers. Pale areas had sparse pigmented cells.

[*]Corresponding author. Department of Ophthalmology and Visual Sciences; EyeSight Foundation of Alabama Vision Research Laboratories, 1670 University Boulevard Room 360; University of Alabama School of Medicine, Birmingham, AL, 35294-0099, USA. christinecurcio@uabmc.edu (C.A. Curcio).

[1]Equal contributions.

Appendix A. Supplementary data

Supplementary data to this article can be found online at https://doi.org/10.1016/j.exer.2021.108882.

Gray areas correlated to cells with RPE organelles entombed in the scar and multinucleate cells containing sparse large spherical melanosomes. In 94% of nvAMD donor eyes, hyperpigmentation was visible. Certain melanotic cells expressed some RPE65 and mostly CD68. Iba1 and TMEM119 immunoreactivity, found both in retina and scar, did not co-localize with melanotic cells.

Conclusion: Hyperpigmentation in CFP results from both organelle content and optical superimposition effects. Black fundus pigment in nvAMD is common and corresponds to cells containing numerous large spherical melanosomes and superimposition of cells containing sparse large melanosomes, respectively. Melanotic cells are molecularly distinct from RPE, consistent with a process of transdifferentiation. The subcellular source of spherical melanosomes remains to be determined. Detailed histology of nvAMD eyes will inform future studies using technologies for spatially resolved molecular discovery to generate new therapies for fibrosis. The potential of black pigment as a biomarker for fibrosis can be investigated in clinical multimodal imaging datasets.

Keywords

Age-related macular degeneration; Color fundus photography; Fibrosis; Histopathology; Melanosomes; Optical coherence tomography; Retinal pigment epithelium

1. Introduction

Fibrosis degrades visual outcomes in eyes with neovascular age-related macular degeneration (nvAMD) receiving anti-vascular endothelial growth factor therapy (Daniel et al., 2013; Ishikawa et al., 2016; Jaffe et al., 2018). Defining the cellular content of fibrotic scars is a key step in exploring new therapeutic targets to potentially reduce or prevent scar formation. New tissue-level techniques that reveal spatially resolved, multiplex molecular composition are becoming available (Anderson et al., 2020; Marx, 2021). Discovery of potential therapeutic targets with these methods can be accelerated by reference to detailed histology of intact donor eyes with nvAMD (Chen et al., 2020a; Curcio et al., 2015; Li et al., 2018a), such as we present herein.

Eyes with nvAMD frequently have black pigment associated with fibrotic scars (62.5% of presenting cases) (De Rosa et al., 2020). Hyperpigmentation, i.e., increased fundus pigment visible by ophthalmoscopy and color fundus photography (CFP), involves several molecularly distinct processes. These include proliferation of retinal pigment epithelial (RPE) cells, enlargement of individual cells, and increased concentration of light-absorbing by larger or more numerous melanin-containing organelles. Melanin in the fundus localizes to organelles of two origins, i.e., melanosomes (from RPE) (Lopes et al., 2007) and melanolipofuscin (components from RPE and photoreceptors) (Feeney, 1978) (Fig. 1). RPE melanosomes are uniquely spindle-shaped (elongated) (Kroll and Machemer, 1968; Pollreisz et al., 2020). Recent counts of human RPE organelles by volumetric microscopy of cells localized precisely with respect to the fovea (Bermond et al., 2020; Pollreisz et al., 2018, 2020) showed that ~2/3 of melanosomes in human macular RPE localize to apical processes. Further, melanosomes are outnumbered by melanolipofuscin even in young adults, and a second population of melanosomes, spherical in shape, may also exist (Bermond et al.,

2020; Pollreisz et al., 2018, 2020). Histologic validation of fundus autofluorescence (FAF) imaging (Chen et al., 2021a, 2021b; Rudolf et al., 2013) has shown that tissue components outside the RPE layer can add to or block signal originating in RPE via optical mechanisms like superimposition and unmasking, independent of the organelle content of individual cells.

Exclusively in nvAMD eyes we described “melanotic cells” packed with large (3–5 μm diameter) spherical melanosomes, distinct from choroidal melanocytes, that were trapped in fibrocellular scars or enveloping subretinal neovascular membranes (Chen et al., 2020a; Zanzottera et al., 2015a, 2015b). Because individual melanotic cells could contain both spindle-shaped and spherical melanosomes, they seemed to result from transdifferentiation of RPE cells without intervening de-differentiation. Further, we recently demonstrated in many abnormal RPE phenotypes a loss of retinoid markers and gain of immune markers. These included anteriorly migrating cells corresponding to hyperreflective foci, progression risk indicators in optical coherence tomography (OCT) (Cao et al., 2021). Independently, RPE transdifferentiation to extracellular matrix-producing cells is considered a route to fibrosis (Shu et al., 2020).

To generate hypotheses about RPE participation in fibrosis, we explored a histologic basis for black pigment in a fibrotic scar secondary to untreated nvAMD. The index eye of our study was pseudophakic, allowing clear fundus visualization over 9 years of follow-up imaging with CFP, FAF, and OCT. To view organelles in melanotic cells and RPE phenotypes, we used high-resolution epoxy resin histology and electron microscopy. In 36 clinically undocumented donor eyes with nvAMD, we assessed the frequency of fundus hyperpigmentation. In three donor eyes with nvAMD, we immunolocalized markers for RPE, macrophages, and microglia. Our results link melanotic cells to black pigment in nvAMD, clarify mechanisms affecting fundus pigment visualization, reveal melanosome-clearing activities, and suggest participation of microglia and macrophages in fibrosis along with RPE.

2. Methods

2.1. Compliance

Retrospective review of medical records and imaging data and histopathology studies were approved by the institutional review boards of the Manhattan Eye, Ear, and Throat Hospital/Northwell Health and the University of Alabama at Birmingham, respectively. All study components complied with the Health Insurance Portability and Accountability Act of 1996 and adhered to the tenets of the Declaration of Helsinki.

2.2. Clinical course of the index eye

Comprehensive ophthalmologic examination and multimodal imaging were performed during a 9-year follow-up of a woman of European descent with inactive subretinal fibrosis due to untreated nvAMD in her right eye. Ocular history included cataract surgery in both eyes. Medical history included chronic obstructive pulmonary disease, gastric cancer, and hypercholesterolemia. There was a 57 pack-year history of smoking. At presentation (age 79

years), CFP (Fig. 2A–D), FAF (Fig. 2E), and fluorescein angiography (Chen et al., 2020b) (Topcon TRC-50IX fundus camera; Topcon, Tokyo, Japan) showed subretinal fibrosis in the right eye and non-exudative type 1 macular neovascularization (MNV) in the left eye. Best-corrected visual acuity was 20/50 in the right eye and 20/25 in the left eye. During follow-up, neither subretinal fluid nor other types of recurrent exudation were detected in the right eye. Neither eye was treated for nvAMD. The diagnosis of nvAMD in both eyes was supported by the presence of drusen and subretinal deposits, and via histology, basal laminar deposit and type 1 neovascularization (Chen et al., 2020b, 2021a, 2021b). This study focuses on the right eye.

At presentation the right eye exhibits on CFP a yellowish central subretinal fibrosis partially rimmed with dark gray pigment (Fig. 2A; details in the Results). At the last registered clinical evaluation (9 years after presentation and 1.3 years before death at age 90), the patient maintained a subretinal fibrosis in the right eye and non-exudative type 1 MNV in the left eye. The subretinal fibrosis was stable in size at the last visit (Fig. 2D). At the same visit, the scar was revealed as deeply hypoautofluorescent (hypoFAF) (Fig. 2E; details in the Results). The left eye at the last clinical visit lacked black pigment or subretinal fibrosis (Fig. 2F). Final best corrected visual acuity was 20/200 and 20/30 in the right and left eyes, respectively.

2.3. Tissue preparation of the index eye

Sixteen months after the last clinical examination, the patient died of complications of chronic obstructive pulmonary disease. Globes were recovered 6.25 h after death by personnel of The Eye-Bank for Sight Restoration (New York USA), opened anteriorly by cornea removal, preserved by immersion in 4% phosphate buffered paraformaldehyde, and shipped overnight on wet ice to Birmingham, Alabama, USA.

An 8 × 12 mm (vertical × horizontal) full-thickness tissue sample including the fovea and most of the optic nerve head was excised from the eyecup, post-fixed with osmium tannic acid paraphenylenediamine to preserve extracellular lipids (Curcio et al., 2001), embedded in epoxy resin (PolyBed 812, EMS, Hatfield PA), and oriented for sectioning in a superior to inferior direction. Glass slides with 0.8 μm-thick sections were stained with toluidine blue (n = 115, distance 64 ± 9 μm, range 25–125 μm). One section per slide was scanned with a 20x objective and a robotic microscope stage (Olympus VSI 120, CellSens; Olympus, Center Valley PA), scaled to tissue units, and centered on the fovea or vertical meridian (where Henle fibers diverge) using a custom plugin for FIJI made available on the ImageJ update site by Creative Computation (https://sites.imagej.net/CreativeComputation/). Selected sections were scanned for detailed review using a 60x oil-immersion objective (numerical aperture = 1.42) and viewed on a monitor at magnifications up to 1240× using FIJI. For figures, images were adjusted to maximize the intensity histogram for contrast and white balance and made into composites (Photoshop CS6, Adobe Systems, USA).

2.4. Histopathologic review of the index eye

For point-by-point OCT-histology correlation, histology sections were referenced to *ex vivo* OCT B-scans, which were in turn referenced to the *in vivo* OCT B-scans from the last clinic

visit, as described (Chen et al., 2020b). Nineteen sections 240 μm apart corresponding to clinical B-scans were used to evaluate pigment variation seen by CFP.

Melanosomes (M), lipofuscin (L), and melanolipofuscin (ML) are lysosome-related organelles (Bowman et al., 2019; Orlow, 1995). Our terminology is based on electron microscopy (Feeney, 1978) and differs from recent studies using the term “granules” to indicate organelles emitting FAF signal, i.e., lipofuscin and melanolipofuscin. Whether melanosomes are a signal source for near-infrared autofluorescence (Keilhauer and Delori, 2006) is under active investigation (Bonilha et al., 2020; Guan et al., 2020; Taubitz et al., 2019).

2.5. Survey of ex vivo CFP from addition donor eyes with nvAMD

To assess the prevalence of black pigment in nvAMD fundus, we surveyed nvAMD eyes at the Project MACULA online resource (Pang et al., 2015; Sura et al., 2020). These eyes were accessioned from donors without ophthalmic history mostly before the anti-VEGF era (2006) and may have been subject to treatments available at that time. Mean death-to-preservation interval was 3:49 h (range = 0:40–11:40 h). For this survey, CFP images acquired with retina in place were assessed for focus quality and visibility of pigmentation. In images of adequate quality, we sought evidence of black or gray retinal pigmentation distinct from choroidal pigmentation.

2.6. Immunohistochemistry of additional donor eyes with nvAMD

Three nvAMD donor eyes with melanotic cells from an independent series were immunoprobed for marker proteins, as described (Cao et al., 2021). Whole eyes were obtained from deceased human donors (≥80 years of age, white, non-diabetic, and ≤6 h death-to-preservation) to the Advancing Sight Network (Birmingham AL USA). Eyes were preserved in 4% buffered paraformaldehyde and screened for AMD presence and stage using *ex vivo* multimodal imaging including OCT, as described (Cao et al., 2021). From 3 eyes with grossly visible nvAMD, 5 × 8 mm rectangles of full-thickness eye wall including fovea and optic nerve were dissected and processed for 12 μm thick cryosections, as described (Cao et al., 2021). For AMD diagnosis, cryosections were stained with periodic acid Schiff hematoxylin to highlight Bruch’s membrane and sub-RPE deposits (Vogt et al., 2011).

Markers for retinoid activity and immune function may be found in cells of RPE origin (Jakobiec et al., 2020). RPE65 (isomerohydrolase of classic visual cycle) (Jin et al., 2005) and CD68 (lysosome marker common in macrophages (Chistiakov et al., 2017)) were localized in bleached and non-bleached sections processed in parallel with an avidin-biotin-peroxidase immunohistochemistry detection system and red reaction product (AEC, 3-amino-9-ethylcarbozole) as described (Cao et al., 2021).

A heat-induced antigen retrieval step comprised steaming slides for 10 min in 1x unmask solution (Vector Labs, #H-3300–250) in glycerol (Fisher, #NC0429714) (Buchwalow and Böcker, 2010) then cooled 20 min and washed with distilled water.

Sections were bleached (Elleder and Borovansky, 2001) (Melanin Kit, Polysciences, Inc. Warrington PA USA, #24883) using solutions A (2.5% potassium permanganate) for 1

min and B (1% ethanedoic acid, commonly called oxalic) for 20 s, each washed with distilled water. Following bleaching, endogenous hydrogen peroxide was quenched and processing proceeded as described (Cao et al., 2021) using primary antibodies of mouse anti-CD68 (1:100, ThermoFisher Scientific, #MA1–80133, Clone #514H12) and mouse anti-RPE65 (1:150, ThermoFisher Scientific, #MA1–16578, Clone #401.8B11.3D9) and isotype negative controls mouse IgG_{2a} (1:1000, ThermoFisher Scientific, #MA1–10418) for CD68 and mouse IgG_{1k} (1:1000, ThermoFisher Scientific, #CBL610, Clone# 1E2.2) for RPE65. Internal positive controls were choroidal macrophages for CD68 and normal RPE cells for RPE65.

To localize microglia in the same tissues, some unbleached sections were stained using primary antibodies for ionized calcium binding adaptor molecule 1 (Iba1; 1:500, Wako, #019–19741) and transmembrane protein 119 (TMEM119; 1:200, Abcam, #ab185333) (Bennett et al., 2016; Su et al., 2019).

Glass slides were scanned using the Olympus system described above and 20x and 40x objectives. RPE morphology was categorized using the Project MACULA grading system (Zanzottera et al., 2015a, 2015b).

3. Results

3.1. Clinical imaging of the index eye

At presentation (11 years before death) the index eye exhibited a yellowish central subretinal fibrotic scar with dark gray pigmented areas along its inferior edge (Fig. 2A). Over 2 years (8.3 years before death), the gray areas darkened and expanded in size and number (Fig. 2B). Thin linear streaks appeared (left of asterisk, Fig. 2B). By 6.6 years after presentation (3.7 years before death, Fig. 2C), pigment coalesced into a dark crescent at the inferior rim of the scar. Three black streaks appeared, of which the most prominent was a diagonally oriented, spear-like extension from the inferior rim towards the center (asterisk, Fig. 2C–E). Closer to the scar center than circumferential zone of black pigment was a zone of gray pigment with focal areas of greenish tinge (Fig. 2C and D). Nine years after presentation (1.3 years before death), FAF imaging (Fig. 2E) revealed a hypoFAF central area larger than the scar, with deepest hypoFAF in the spear-like extension (asterisk, Fig. 2E). Outside the fibrotic scar pigmentary changes were observed in association with drusen. After death (11 years after presentation and 16 months after the last clinical visit), *ex vivo* CFP confirmed that the pigment distribution was virtually unchanged (Supplementary Fig. 1).

3.2. Histologic analysis of the index eye

We next show cells containing melanosomes in the central fibrotic area, all located internal to persistent BLamD and thus considered subretinal (as opposed to sub-RPE) (Zanzottera et al., 2016). Fig. 3 links an OCT B-scan through the fibrotic scar from the last clinical visit to histology. Hyperreflective lesions correspond to black pigment visible on CFP and outer retinal tubulation (ORT) that is invisible by CFP (Fig. 3A). The fibrotic scar, melanotic cells, and ORT corresponding to the OCT B-scan (Fig. 3B) are apparent in the tissue section (Fig. 3C).

By CFP, we identified 7 zones with different degrees of melaninization, presented in order from temporal to nasal (left to right in Fig. 3A and C). A black pigmented area (Fig. 3D) has a low mound of rounded melanotic cells with densely packed spherical melanosomes of uniform diameter. A gray pigmented area (Fig. 3E) shows reduplicated collagen mixed with multinucleate cells containing scattered dark spherical organelles. In this same area, singular and aggregated melanosomes are found within overlying neurosensory retina. A black spear-shaped area (Fig. 3F, asterisk) has melanotic cells with dense dark spherical melanosomes lying above fibrocellular membranes. In a pale-yellow zone (Fig. 3G), melanosomes are sparse. A gray pigmented zone (Fig. 3H) has a single layer of RPE entombed between lamellae of fibrovascular scars (Zanzottera et al., 2015b). A third zone of black pigment (Fig. 3I) has two layers of melanotic cells. A depigmented yellow zone (Fig. 3J) corresponds to macular atrophy with persistent BLamD, a few scattered RPE granules, and cellular processes in sub-RPE-basal lamina (BL) space.

Fig. 4 shows variation in melanosome morphology by electron microscopy. Fig. 5 shows variation in melanosome packing by light microscopy at the fundus levels in Supplementary Figure 2). Spindle-shaped melanosomes are the native RPE organelle (Figs. 4A and 5A). Infrequently found in this advanced AMD eye, native melanosomes are uniformly electron dense. They are distinguishable from both lipofuscin (moderate and uniform electron density) and melanolipofuscin (dense with fibrillar internal structure, Fig. 4A). Large spherical melanosomes with regularly spaced pits along the surface are densely packed in melanotic cells (Fig. 4B and 5 B,C). In contrast to RPE melanosomes, melanosomes within choroidal melanocytes are spherical, very small, and densely packed (Figs. 4C and 5I). Entombed RPE have both spindle-shaped (Fig. 5 E andG) and spherical melanosomes (0.3–3.5 μm diameter, Fig. 5E and F). Rounded cells inside ORT, believed to originate from RPE that detached from the layer, have sparse spindle-shaped and spherical melanosomes (Fig. 5H). Cells clearing debris are suggested by scattered large melanosomes in multinucleate giant cells (Ooto et al., 2014; Penfold et al., 1986) (Fig. 5D), spherical melanosomes packed around a nucleus, presumably within a cell body (Fig. 5G), and spindle-shaped melanosomes within Müller glia (Fig. 6).

3.3. Survey of ex vivo CFP from additional nvAMD donor eyes

Of nvAMD donor eyes on the Project MACULA website, 36 had gradable *ex vivo* CFP imaging, as exemplified by 3 eyes in Fig. 7. Of these, 34 (94%) had black pigment in a fibrotic scar, ranging from small (Fig. 7A) to extensive and branching (Fig. 7B and C).

3.4. Immunohistochemistry of additional nvAMD donor eyes

Three nvAMD donor eyes with melanotic cells, from an independent series, were immunoprobed for marker proteins RPE65 and CD68 (Fig. 8). Visibility of reaction product was aided by bleaching nearby sections in the same fundus area (compare unbleached in Fig. 8A, C, E, G, I) to bleached in Fig. 8B, D, F, H, J). Sections with normal and ectopic RPE served as positive controls (Fig. 8K–L). Sections with normal RPE and choroidal macrophages served as antibody isotype controls (Fig. 8M–N).

RPE65, the isomerohydrolase of the classic visual cycle, is expressed by normal RPE and is not expressed by abnormal phenotypes (Fig. 8K–L) (Cao et al., 2021). CD68 is a lysosomal protein expressed in choroidal macrophages (positive controls) and in fully pigmented cells sloughed from the RPE layer and not in normal cells (Cao et al., 2021) (Fig. 8K–L). Some melanotic cells with moderate levels of spherical melanosomes are immunoreactive for each of these two markers (Fig. 8C,D,E,F). Fewer heavily pigmented cells exhibit immunoreactivity for these markers than the moderately pigmented cells (Fig. 8G,H,I,J). Melanotic cells exhibit less intense signal for RPE65 (Fig. 8D) than entombed RPE, which contains characteristic RPE organelles (Zanzottera et al., 2015a).

Microglial cells are immune surveillance cells that reside in inner retina and migrate to outer retina in conditions of photoreceptor injury. To determine if microglia are present near cells containing spherical melanosomes, these same nvAMD eyes were immunoprobed for Iba1 and TMEM119 (Fig. 9). and compared to negative control sections (Fig. 9D and E). In the same eye as that shown in Fig. 8G–J, immunoreactivity for Iba1 and TMEM119 (Fig. 9A and B, respectively) localizes to fibrotic tissue between melanotic cells as well as resident macrophages in the choroid. In Fig. 9B, signal for TMEM119 is stronger overall and additionally localizes to overlying retina, in which both ONL and HFL are degenerated. Also, the same eye as that shown in Fig. 8G–J, a multinucleate complex containing spherical melanosomes is not TMEM119 immunoreactive (Fig. 9C). Due to insufficient tissue sections, it was not possible to test for Iba1 in this complex.

4. Discussion

In the index eye, areas of black hyperpigmentation are non-autofluorescent and attributable to both RPE-cell-autonomous effects and optical effects involving superimposition of melanosome-containing cells. The blackest areas correlated to melanotic cells, some in multiple layers, appearing slowly over time, and persisting. Pale areas had sparse pigmented cells and debris and exhibited slight FAF signal, possibly from the scar itself. Gray areas correlated to cells entombed within scars containing a moderate load of typical RPE organelles and to multinucleate giant cells with scattered large melanosomes. Melanotic cells are morphologically and molecularly distinct from normal RPE and do not exhibit common markers for microglia.

Black pigment is common in nvAMD, and our direct observation of retina without obscuration by age-related anterior segment opacities suggests an even higher frequency than seen clinically (De Rosa et al., 2020). Our data may be compared to black fundus pigment appearing in other conditions involving RPE disturbances, such as macular telangiectasia type 2 (Leung et al., 2018) and in bone spicule degeneration of retinitis pigmentosa. In the latter, RPE cells with spherical melanosomes and lacking immunoreactivity for retinoid marker cellular retinaldehyde binding protein migrate anteriorly and wrap around peripheral retinal blood vessels (Jaissle et al., 2010; Li et al., 1995). RPE transplantation trials for AMD exhibited post-operative hyperpigmentation (da Cruz et al., 2018; Kashani et al., 2018; Schwartz et al., 2012; Schwartz et al., 2014; Song et al., 2015) that was considered abnormal (Kashani et al., 2020) and in pre-clinical transplantation studies (Cho et al., 2019; Liu et al., 2020; McGill et al., 2018), black

pigment was found by histology. High-resolution histology of eyes with transplants will help determine if these findings are related.

By electron microscopy, melanosomes in melanotic cells in the index eye could be distinguished from those in other cells. These non-autofluorescent organelles appeared uniformly electron-dense with regularly spaced pits on their surface (Fig. 5A), resembling mature melanosomes (Feeney, 1978). Melanotic cell melanosomes are more numerous and densely packed than the characteristic spindle-shaped melanosomes of normal RPE. The latter were rarely found in our sample, due to severity of disease and damage to apical processes by post-mortem detachment. Only spherical melanosomes were seen in ultrastructural studies of congenital hypertrophy of RPE (Lloyd et al., 1990), bone spicule degeneration in retinitis pigmentosa (Li et al., 1995) and peripheral RPE of aged monkey (Gouras et al., 2018), possibly due to real differences in melaninization, absence of apical processes, or both.

Our data suggest that one source of melanotic cells is native RPE, originating either within the scar or, less likely, from less affected tissue surrounding the scar. We did not observe mitotic figures suggestive of cell division in the index eye or any others prepared and viewed with the same methods. Transdifferentiation is the conversion of one differentiated cell type to another, without an intervening state of dedifferentiation and proliferation. Consistent with this idea, our published histologic survey of 41 nvAMD eyes demonstrated sheets of RPE cells trapped between layers of fibrovascular tissue (“entombed”) (Zanzottera et al., 2015a), with individual cells containing both spindle-shaped and spherical melanosomes. In type 2 (subretinal) MNV RPE envelops the MNV, and we previously observed a smooth transition within the enveloping RPE layer from cells containing age-normal organelles to those containing spherical melanosomes (Chen et al., 2020a). As shown previously for ectopic pigmented cells (Jakobiec et al., 2020) we herein found that some melanotic cells are immunoreactive for RPE65 but most are not (Fig. 8), again consistent with a transition and also casting doubt that these cells could support vision, even if photoreceptors were present. We were aided in our assessments by detailed comprehensive photomicroscopy of bleached and non-bleached cells to reveal melanosomes in labeled and unlabeled cells (Fig. 8). We previously used full pigmentation as evidence that hyperreflective foci, an OCT biomarker for progression risk in AMD (Ouyang et al., 2013; Sadda et al., 2020), were intraretinal RPE cells (Balaratnasingam et al., 2017; Cao et al., 2021; Li et al., 2018a) Melanotic cells are long-lasting, but if RPE65 status is an indicator, they would not perform a full range of expected RPE functions.

A stimulus for conversion of RPE to melanotic cells is unknown but may be contact with other cells capable of inducing transdifferentiation. Both in the index eye and in our previous histologic survey melanotic cells were found in fibrotic scars internal to persistent BLamD (Zanzottera et al., 2016). In the index eye, we observed that hyperpigmentation expanded only within the scar (Fig. 1), which contains fibroblasts and vascular cells. Other possible inducers include activated Müller glia as seen in our prior published case (Chen et al., 2020a), and circulating cells and factors that transudate.

Although we showed that immunoreactivity for microglial markers did not colocalize with melanotic cells, we cannot completely exclude phagocytes that ingested and retained characteristic RPE organelles as cells of origin. Phagocytes are distinguished by phagolysosomes, i.e., cytoplasmic vacuoles formed by the fusion of phagosomes containing ingested material with lysosomes. We did not see phagolysosomes by previous electron microscopic analysis of pigmented intraretinal cells corresponding to hyperreflective foci (Chen et al., 2016), nor did we see them here (Fig. 5). We did demonstrate in bleached melanotic cells (as well as in sloughed cells) immunoreactivity for CD68, a lysosomal membrane protein reliably found in macrophages of myeloid origin (Chistiakov et al., 2017). We emphasize that expression of CD68 detected at one time point does not indicate that melanotic cells originated as macrophages or assumed macrophage behavior, nor does it imply that macrophages of hematopoietic origin known from prior research to be present in choroid and sub-RPE-BL space (Cherepanoff et al., 2010; McLeod et al., 2016) actually started as RPE. One unlikely source of melanotic cells is choroidal melanocytes, which have small and densely packed melanosomes. No evidence yet indicates melanocytes in type 1 MNV (of choroidal origin) (Grossniklaus et al., 2005). Further, melanosomes in RPE and choroidal melanocytes differ in genetic regulation and developmental time course (Lopes et al., 2007; Nir et al., 1995).

We provide evidence that gray pigmentation in the fundus may result from dispersion of melanosomes by non-RPE cell types. Multinucleated giant cells form by fusion of monocytes in numerous disorders (Brooks et al., 2019). Of possible relevance to very large melanosomes observed in nvAMD (Fig. 4) (Ooto et al., 2014; Penfold et al., 1986), giant cells in foreign body reactions ingest material too large for other phagocytes (Brooks et al., 2019). We previously found spindle-shaped and spherical melanosomes within the Henle fiber layer depleted of photoreceptors (Li et al., 2018b; Tan et al., 2018), implying ingestion by Müller glia, herein confirmed by electron microscopy (Fig. 6). To these, we also add small cell bodies suggestive of microglia (Fig. 4G) as seen by others (Chen et al., 2021a; Ma et al., 2013). Evidence that a melanosome life cycle is visible in the fundus (Figs. 2 and 3) supports conclusions from the first-in-human RPE transplant trial (Schwartz et al., 2012, 2014). These authors stated that post-operative subretinal hyperpigmentation might not represent transplanted RPE, but rather, phagocytes that ingested pigment, and thus RPE cell functionality cannot be assessed by pigmentation alone. A combination of FAF and OCT to assess both the potential for disk renewal and optical effects from non-RPE layers, respectively, is recommended.

Our data do not elucidate what organelles give rise to spherical melanosomes. Experimental studies suggest that after birth RPE melanogenesis continues at a low level compared to other ocular pigmented cells (Lindquist et al., 1998; Lopes et al., 2007). Models of melanolipofuscin biogenesis invoke fusion of one or both melanosome types with pre-existing lysosomes and dissolution of melanin, and expansion of a small autofluorescent component in melanosomes over time (Bermond et al., 2020; Feeney, 1978; Warburton et al., 2007). We did not see lobular macro-melanosomes formed by fusion of smaller organelles (Storm et al., 2019). Advanced nano-analytic assays detect nitrogen and phosphorus within all components of melanolipofuscin (Taubitz et al., 2019). Because of this admixing and the abundance of lipofuscin and melanolipofuscin in our sample, they are

both possible precursors of melanosomes in melanotic cells, implying an unexpected level of dynamism for these organelles.

Strengths of this study include a well-documented pseudophakic eye with untreated nvAMD, documented with long follow-up and highquality multimodal imaging, high-resolution comprehensive histology, photomicroscopy, and electron microscopy, and clear immunoreactivity signals. Limitations of the clinicopathologic correlation include lack of history of neovascularization and melanization onset and lack of near-infrared FAF imaging for melanin (Keilhauer and Delori, 2006). Limitations of the donor eye studies include lack of double-labeling to identify transdifferentiating cells (Jakobiec et al., 2020) and lack of non-osmicated samples to distinguish melanosomes from lipofuscin and melanolipofuscin (Burns and Feeney-Burns, 1980; Gouras et al., 2018). Our data do not resolve whether the expansion of black fundus pigmentation (Fig. 1) is due to cell proliferation, failure of cell death and clearing mechanisms, or hypertrophy of individual cells. Our data do not exclude the possibility of RPE transdifferentiation to extracellular matrix-producing cells in fibrosis (Shu et al., 2020).

Despite these limitations, our description of black fundus pigment in nvAMD can assist several future directions. Our data will aid interpretation of CFP especially with the advent of OCT technologies with sufficient axial resolution to resolve RPE details (Lee et al., 2020; Shirazi et al., 2020; Zhang et al., 2019) (Fig. 1) and instruments capable of both CFP and OCT imaging (Corradetti et al., 2021). The intriguing possibility that black pigmentation is a biomarker for fibrosis depends on whether melanotic cells are a response to fibrosis or an instigating event. This question is potentially addressable by analyzing clinical trial imaging datasets including CFP and OCT. Our observations can also assist the interpretation of imaging outcomes in trials for RPE replacement therapies. Finally, detailed histology is helpful for interpreting spatially-resolved, multiplex molecular composition in complex AMD tissues, as is now technically feasible (Anderson et al., 2020; Marx, 2021).

Supplementary Material

Refer to Web version on PubMed Central for supplementary material.

Acknowledgments

We thank The Eye-Bank for Sight Restoration (NYC) for timely retrieval of eyes from the clinically characterized donor and Advancing Sight Network (Birmingham AL) for timely retrieval of eyes used for Project MACULA and for the immunohistochemistry described herein.

Financial support

Supported by Genentech/Hoffman LaRoche, Heidelberg Engineering, The Macula Foundation, Inc., New York, NY; unrestricted funds to the Department of Ophthalmology and Visual Sciences (UAB) from Research to Prevent Blindness, Inc., and EyeSight Foundation of Alabama. Acquisition of human tissues for immunohistochemistry was funded by NIH grant R01EY015520 (CAC) and R01EY027948 (CAC, TA) and IZKF Würzburg (N-304, TA). The Project MACULA website and recovery of human donor eyes for research was supported by NIH grants R01EY06019 and P30 EY003039, EyeSight Foundation of Alabama, International Retinal Research Foundation, Edward N. and Della L. Thome Foundation, the Arnold and Mabel Beckman Initiative for Macular Research, and Research to Prevent Blindness Inc.

Financial disclosure

KBF is a consultant to Genentech, Regeneron, Zeiss, Heidelberg Engineering, Allergan, and Novartis. CAC receives research funds from Genentech/Hoffman LaRoche and Heidelberg Engineering and is a stockholder of MacRegen Inc. DF is an employee of Genentech and has stock/stock options of Roche. TA is a consultant to Novartis, Roche, Heidelberg Engineering and receives funds from Novartis and Nidek and is a stockholder of MacRegen Inc.

Abbreviations

AMD	age-related macular degeneration
BLamD	basal laminar deposit
BrM	Bruch's membrane
CFP	color fundus photographs
ChC	choriocapillaris
Ch	choroid
ELM	external limiting membrane
FAF	fundus autofluorescence
Fs	fibrotic scar
GCL	ganglion cell layer
HFL	Henle fiber layer
HFL/ONL	dyslamination of HFL and ONL
Iba1	ionized calcium binding adaptor molecule 1
INL	inner nuclear layer
IPL	inner plexiform layer
IS	inner segment
M	melanosomes
MNV	macular neovascularization
ML	melanolipofuscin
L	lipofuscin
nvAMD	neovascular age-related macular degeneration
OCT	optical coherence tomography
OPL	outer plexiform layer
OS	outer segment

RPE	retinal pigment epithelium
TMEM119	transmembrane protein 119

References

Anderson DMG, Messinger JD, Patterson NH, Rivera ES, Kotnala A, Spraggins JM, Caprioli RM, Curcio CA, Schey KL, 2020. The molecular landscape of the human retina and supporting tissues by high resolution imaging mass spectrometry. J. Am. Soc. Mass Spectrom 31, 2426–2436. [PubMed: 32628476]

Balaratnasingam C, Messinger JD, Sloan KR, Yannuzzi LA, Freund KB, Curcio CA, 2017. Histologic and optical coherence tomographic correlations in drusenoid pigment epithelium detachment in age-related macular degeneration. Ophthalmology 124, 644–656. [PubMed: 28153442]

Bennett ML, Bennett FC, Liddelow SA, Ajami B, Zamanian JL, Fernhoff NB, Mulinyawe SB, Bohlen CJ, Adil A, Tucker A, Weissman IL, Chang EF, Li G, Grant GA, Hayden Gephart MG, Barres BA, 2016. New tools for studying microglia in the mouse and human CNS. Proc. Natl. Acad. Sci. U. S. A 113, E1738–E1746. [PubMed: 26884166]

Bermond K, Wobbe C, Tarau IS, Heintzmann R, Hillenkamp J, Curcio CA, Sloan KR, Ach T, 2020. Autofluorescent granules of the human retinal pigment epithelium: age-related topographic and intracellular distribution. Invest. Ophthalmol. Vis. Sci 61, 35.

Bonilha VL, Bell BA, Hu J, Milliner C, Pauer GJ, Hagstrom SA, Radu RA, Hollyfield JG, 2020. Geographic atrophy: confocal scanning laser ophthalmoscopy, histology, and inflammation in the region of expanding lesions. Invest. Ophthalmol. Vis. Sci 61, 15.

Bowman SL, Bi-Karchin J, Le L, Marks MS, 2019. The road to lysosome-related organelles: insights from Hermansky-Pudlak syndrome and other rare diseases. Traffic 20, 404–435. [PubMed: 30945407]

Brooks PJ, Glogauer M, McCulloch CA, 2019. An overview of the derivation and function of multinucleated giant cells and their role in pathologic processes. Am. J. Pathol 189, 1145–1158. [PubMed: 30926333]

Buchwalow IB, Böcker W, 2010. Immunohistochemistry: Basic and Methods. Springer-Verlag, Berlin.

Burns RP, Feeney-Burns L, 1980. Clinico-morphologic correlations of drusen of Bruch's membrane. Trans. Am. Ophthalmol. Soc 78, 206–225. [PubMed: 6167054]

Cao D, Leong B, Messinger JD, Kar D, Ach T, Yannuzzi LA, Freund KB, Curcio CA, 2021. Hyperreflective foci, OCT progression indicators in age-related macular degeneration, include transdifferentiated retinal pigment epithelium. Invest. Ophthalmol. Vis. Sci 62, 34.

Chen KC, Jung JJ, Curcio CA, Balaratnasingam C, Gallego-Pinazo R, Dolz-Marco R, Freund KB, Yannuzzi LA, 2016. Intraretinal hyperreflective foci in acquired vitelliform lesions of the macula: clinical and histologic study. Am. J. Ophthalmol 164, 89–98. [PubMed: 26868959]

Chen L, Li M, Messinger JD, Ferrara D, Curcio CA, Freund KB, 2020a. Recognizing atrophy and mixed-type neovascularization in age-related macular degeneration via clinicopathologic correlation. Transl Vis Sci Technol 9, 8.

Chen L, Messinger JD, Ferrara D, Freund KB, Curcio CA, 2021a. Fundus autofluorescence in neovascular age-related macular degeneration, a clinicopathologic correlation relevant to macular atrophy. Ophthalmology Retina 5, 1085–1096. [PubMed: 33540168]

Chen L, Messinger JD, Ferrara D, Freund KB, Curcio CA, 2021b. Stages of drusen-associated atrophy in age-related macular degeneration visible via histologically validated fundus autofluorescence. Ophthalmology Retina 5, 730–742. [PubMed: 33217617]

Chen L, Messinger JD, Sloan KR, Swain TA, Sugiura Y, Yannuzzi LA, Curcio CA, Freund KB, 2020b. Non-exudative neovascularization supporting outer retina in age-related macular degeneration, a clinicopathologic correlation. Ophthalmology 127, 931–947. [PubMed: 32247535]

Cherepanoff S, McMenamin PG, Gillies MC, Kettle E, Sarks SH, 2010. Bruch's membrane and choroidal macrophages in early and advanced age-related macular degeneration. Br. J. Ophthalmol 94, 918–925. [PubMed: 19965817]

Chistiakov DA, Killingsworth MC, Myasoedova VA, Orekhov AN, Bobryshev YV, 2017. CD68/macrosialin: not just a histochemical marker. Lab. Invest 97, 4–13.

Cho SM, Lee J, Lee HB, Choi HJ, Ryu JE, Lee HJ, Park HK, Lee MJ, Lee J, Lee H, Kim HS, Lee JY, Son WC, 2019. Subretinal transplantation of human embryonic stem cell-derived retinal pigment epithelium (MA09-hRPE): a safety and tolerability evaluation in minipigs. Regul. Toxicol. Pharmacol

Corradetti G, Byon I, Corvi F, Cozzi M, Staurenghi G, Sadda SR, 2021. Retro mode illumination for detecting and quantifying the area of geographic atrophy in non-neovascular age-related macular degeneration. Eye.

Curcio CA, Balaratnasingam C, Messinger JD, Yannuzzi LA, Freund KB, 2015. Correlation of type 1 neovascularization associated with acquired vitelliform lesion in the setting of age-related macular degeneration. Am. J. Ophthalmol 160, 1024–1033 e1023. [PubMed: 26255578]

Curcio CA, Millican CL, Bailey T, Kruth HS, 2001. Accumulation of cholesterol with age in human Bruch's membrane. Invest. Ophthalmol. Vis. Sci 42, 265–274. [PubMed: 11133878]

da Cruz L, Fynes K, Georgiadis O, Kerby J, Luo YH, Ahmado A, Vernon A, Daniels JT, Nommiste B, Hasan SM, Gooljar SB, Carr AF, Vugler A, Ramsden CM, Bictash M, Fenster M, Steer J, Harbinson T, Wilbrey A, Tufail A, Feng G, Whitlock M, Robson AG, Holder GE, Sagoo MS, Loudon PT, Whiting P, Coffey PJ, 2018. Phase 1 clinical study of an embryonic stem cell-derived retinal pigment epithelium patch in age-related macular degeneration. Nat. Biotechnol

Daniel E, Toth CA, Grunwald JE, Jaffe GJ, Martin DF, Fine SL, Huang J, Ying GS, Hagstrom SA, Winter K, Maguire MG, 2013. Risk of scar in the comparison of age-related macular degeneration treatments trials. Ophthalmology 121, 656–666. [PubMed: 24314839]

De Rosa I, Ohayon A, Semoun O, Miere A, Jung C, Capuano V, Cirafici P, Souied EH, 2020. Real-color versus pseudo-color imaging of fibrotic scars in exudative age-related macular degeneration. Retina 40, 2277–2284. [PubMed: 32039941]

Elleder M, Borovansky J, 2001. Autofluorescence of melanins induced by ultraviolet radiation and near ultraviolet light. A histochemical and biochemical study. Histochem. J 33, 273–281. [PubMed: 11563540]

Feeney L, 1978. Lipofuscin and melanin of human retinal pigment epithelium. Fluorescence, enzyme cytochemical and ultrastructural studies. Invest. Ophthalmol. Vis. Sci 17, 583–600. [PubMed: 669890]

Gouras P, Brown KR, Mattison JA, Neuringer M, Nagasaki T, Ivert L, 2018. The ultrastructure, spatial distribution, and osmium tetroxide binding of lipofuscin and melanosomes in aging monkey retinal epithelium. Curr. Eye Res 43, 1019–1023. [PubMed: 29641909]

Grossniklaus HE, Miskala PH, Green WR, Bressler SB, Hawkins BS, Toth C, Wilson DJ, Bressler NM, 2005. Histopathologic and ultrastructural features of surgically excised subfoveal choroidal neovascular lesions: submacular surgery trials report no. 7. Arch. Ophthalmol 123, 914–921. [PubMed: 16009831]

Guan Z, Li Y, Jiao S, Yeasmin N, Rosenfeld PJ, Dubovy SR, Lam BL, Wen R, 2020. A2E distribution in RPE granules in human eyes. Molecules 25.

Ishikawa K, Kannan R, Hinton DR, 2016. Molecular mechanisms of subretinal fibrosis in age-related macular degeneration. Exp. Eye Res 142, 19–25. [PubMed: 25773985]

Jaffe GJ, Ying GS, Toth CA, Daniel E, Grunwald JE, Martin DF, Maguire MG, Comparison of Age-related Macular Degeneration Treatments Trials Research, G., 2018. Macular morphology and visual acuity in year five of the comparison of age-related macular degeneration treatments trials (CATT). Ophthalmology.

Jaissle GB, May CA, van de Pavert SA, Wenzel A, Claes-May E, Giessl A, Szurman P, Wolfrum U, Wijnholds J, Fischer MD, Humphries P, Seeliger MW, 2010. Bone spicule pigment formation in retinitis pigmentosa: insights from a mouse model. Graefes Arch. Clin. Exp. Ophthalmol 248, 1063–1070. [PubMed: 20012642]

Jakobiec FA, Barrantes PC, Yonekawa Y, Lad EM, Proia AD, 2020. Subretinal mononuclear cells in Coats' disease studied with RPE65 and CD163: evidence for histiocytoid pigment epithelial cells. Am. J. Ophthalmol 222, 388–396. [PubMed: 32950512]

Jin M, Li S, Moghrabi WN, Sun H, Travis GH, 2005. Rpe65 is the retinoid isomerase in bovine retinal pigment epithelium. Cell 122, 449–459. [PubMed: 16096063]

Kashani AH, Lebkowski JS, Rahhal FM, Avery RL, Salehi-Had H, Dang W, Lin CM, Mitra D, Zhu D, Thomas BB, Hikita ST, Pennington BO, Johnson LV, Clegg DO, Hinton DR, Humayun MS, 2018. A bioengineered retinal pigment epithelial monolayer for advanced, dry age-related macular degeneration. Sci. Transl. Med 10.

Kashani AH, Uang J, Mert M, Rahhal F, Chan C, Avery RL, Dugel P, Chen S, Lebkowski J, Clegg DO, Hinton DR, Humayun MS, 2020. Surgical method for implantation of a biosynthetic retinal pigment epithelium monolayer for geographic atrophy: experience from a phase 1/2a study. Ophthalmol Retina 4, 264–273. [PubMed: 31786135]

Keilhauer CN, Delori FC, 2006. Near-infrared autofluorescence imaging of the fundus: visualization of ocular melanin. Invest. Ophthalmol. Vis. Sci 47, 3556–3564. [PubMed: 16877429]

Kroll AJ, Machemer R, 1968. Experimental retinal detachment in the owl monkey. 3. Electron microscopy of retina and pigment epithelium. Am. J. Ophthalmol 66, 410–427. [PubMed: 4970987]

Lee B, Chen S, Moult EM, Yu Y, Alibhai AY, Mehta N, Baumal CR, Waheed NK, Fujimoto JG, 2020. High-speed, ultrahigh-resolution spectral-domain OCT with extended imaging range using reference arm length matching. Translational Vision Science & Technology 9, 12–12.

Leung I, Sallo FB, Bonelli R, Clemons TE, Pauleikhoff D, Chew EY, Bird AC, Peto T, MacTel Study G, 2018. Characteristics of pigmented lesions in type 2 idiopathic macular telangiectasia. Retina 38 (Suppl. 1), S43–S50. [PubMed: 29095354]

Li M, Dolz-Marco R, Messinger JD, Wang L, Feist RM, Girkin CA, Gattoussi S, Ferrara D, Curcio CA, Freund KB, 2018a. Clinicopathologic correlation of anti-vascular endothelial growth factor-treated type 3 neovascularization in age-related macular degeneration. Ophthalmology 125, 276–287. [PubMed: 28964579]

Li M, Huisingh C, Messinger JD, Dolz-Marco R, Ferrara D, Freund KB, Curcio CA, 2018b. Histology of geographic atrophy secondary to age-related macular degeneration: a multilayer approach. Retina 38, 1937–1953. [PubMed: 29746415]

Li Z-Y, Possin DE, Milam AH, 1995. Histopathology of bone spicule pigmentation in retinitis pigmentosa. Ophthalmology 102, 805–816. [PubMed: 7777280]

Lindquist NG, Larsson BS, Stjernschantz J, Sjoquist B, 1998. Age-related melanogenesis in the eye of mice, studied by microautoradiography of 3H-methimazole, a specific marker of melanin synthesis. Exp. Eye Res 67, 259–264. [PubMed: 9778406]

Liu Z, Parikh BH, Tan QSW, Wong DSL, Ong KH, Yu W, Seah I, Holder GE, Hunziker W, Tan GSW, Barathi VA, Lingam G, Stanzel BV, Blenkinsop TA, Su X, 2020. Surgical transplantation of human RPE stem cell-derived RPE monolayers into non-human primates with immunosuppression. Stem Cell Reports

Lloyd WC 3rd, Eagle RC Jr., Shields JA, Kwa DM, Arbizo VV, 1990. Congenital hypertrophy of the retinal pigment epithelium. Electron microscopic and morphometric observations. Ophthalmology 97, 1052–1060. [PubMed: 2402417]

Lopes VS, Wasmeier C, Seabra MC, Futter CE, 2007. Melanosome maturation defect in Rab38-deficient retinal pigment epithelium results in instability of immature melanosomes during transient melanogenesis. Mol. Biol. Cell 18, 3914–3927. [PubMed: 17671165]

Ma W, Coon S, Zhao L, Fariss RN, Wong WT, 2013. A2E accumulation influences retinal microglial activation and complement regulation. Neurobiol. Aging 34, 943–960. [PubMed: 22819137]

Marx V, 2021. Method of the Year: spatially resolved transcriptomics. Nat. Methods 18, 9–14. [PubMed: 33408395]

McGill TJ, Stoddard J, Renner LM, Messaoudi I, Bharti K, Mitalipov S, Lauer A, Wilson DJ, Neuringer M, 2018. Allogeneic iPSC-derived RPE cell graft failure following transplantation into the subretinal space in nonhuman primates. Invest. Ophthalmol. Vis. Sci 59, 1374–1383. [PubMed: 29625461]

McLeod DS, Bhutto I, Edwards MM, Silver RE, Seddon JM, Lutty GA, 2016. Distribution and quantification of choroidal macrophages in human eyes with age-related macular degeneration. Invest. Ophthalmol. Vis. Sci 57, 5843–5855. [PubMed: 27802514]

Nir I, Ransom N, Smith SB, 1995. Ultrastructural features of retinal dystrophy in mutant vitiligo mice. Exp. Eye Res 61, 363–377. [PubMed: 7556499]

Ooto S, Vongkulsiri S, Sato T, Suzuki M, Curcio CA, Spaide RF, 2014. Outer retinal corrugations in age-related macular degeneration. JAMA Ophthalmol 132, 806–813. [PubMed: 24801396]

Orlow SJ, 1995. Melanosomes are specialized members of the lysosomal lineage of organelles. J. Invest. Dermatol 105, 3–7. [PubMed: 7615972]

Ouyang Y, Heussen FM, Hariri A, Keane PA, Sadda SR, 2013. Optical coherence tomography-based observation of the natural history of drusenoid lesion in eyes with dry age-related macular degeneration. Ophthalmology 120, 2656–2665. [PubMed: 23830761]

Pang C, Messinger JD, Zanzottera EC, Freund KB, Curcio CA, 2015. The Onion Sign in neovascular age-related macular degeneration represents cholesterol crystals. Ophthalmology 122, 2316–2326. [PubMed: 26298717]

Penfold PL, Killingsworth MC, Sarks SH, 1986. Senile macular degeneration. The involvement of giant cells in atrophy of the retinal pigment epithelium. Invest. Ophthalmol. Vis. Sci 27, 364–371. [PubMed: 3949464]

Pollreisz A, Messinger JD, Sloan KR, Mittermueller T, Weinhandl AS, Benson E, Kidd GJ, Schmidt-Erfurth U, Curcio CA, 2018. Visualizing melanosomes, lipofuscin, and melanolipofuscin in human retinal pigment epithelium using serial block face scanning electron microscopy. Exp. Eye Res 166, 131–139. [PubMed: 29066281]

Pollreisz A, Neschi M, Sloan KR, Pircher M, Mittermueller TJ, Dacey DM, Schmidt-Erfurth U, Curcio CA, 2020. An atlas of human retinal pigment epithelium organelles significant for clinical imaging. Invest. Ophthalmol. Vis. Sci 61, 13.

Rudolf M, Vogt SD, Curcio CA, Huisingh C, McGwin G Jr., Wagner A, Grisanti S, Read RW, 2013. Histologic basis of variations in retinal pigment epithelium autofluorescence in eyes with geographic atrophy. Ophthalmology 120, 821–828. [PubMed: 23357621]

Sadda SR, Abdelfattah NS, Lei J, Shi Y, Marion KM, Morgenthien E, Gune S, Balasubramanian S, 2020. Spectral-domain OCT analysis of risk factors for macular atrophy development in the HARBOR Study for neovascular age-related macular degeneration. Ophthalmology 127, 1360–1370. [PubMed: 32402555]

Schaal KB, Freund KB, Litts KM, Zhang Y, Messinger JD, Curcio CA, 2015. Outer retinal tubulation in advanced age-related macular degeneration: optical coherence tomographic findings correspond to histology. Retina 35, 1339–1350. [PubMed: 25635579]

Schwartz SD, Hubschman JP, Heilwell G, Franco-Cardenas V, Pan CK, Ostrick RM, Mickunas E, Gay R, Klimanskaya I, Lanza R, 2012. Embryonic stem cell trials for macular degeneration: a preliminary report. Lancet 379, 713–720. [PubMed: 22281388]

Schwartz SD, Regillo CD, Lam BL, Eliott D, Rosenfeld PJ, Gregori NZ, Hubschman JP, Davis JL, Heilwell G, Spirn M, Maguire J, Gay R, Bateman J, Ostrick RM, Morris D, Vincent M, Anglade E, Del Priore LV, Lanza R, 2014. Human embryonic stem cell-derived retinal pigment epithelium in patients with age-related macular degeneration and Stargardt's macular dystrophy: follow-up of two open-label phase 1/2 studies. Lancet 385, 509–516. [PubMed: 25458728]

Shirazi MF, Brunner E, Laslandes M, Pollreisz A, Hitzenberger CK, Pircher M, 2020. Visualizing human photoreceptor and retinal pigment epithelium cell mosaics in a single volume scan over an extended field of view with adaptive optics optical coherence tomography. Biomed. Opt Express 11, 4520–4535. [PubMed: 32923061]

Shu DY, Butcher E, Saint-Geniez M, 2020. EMT and EndMT: emerging roles in age-related macular degeneration. Int. J. Mol. Sci 21.

Song WK, Park KM, Kim HJ, Lee JH, Choi J, Chong SY, Shim SH, Del Priore LV, Lanza R, 2015. Treatment of macular degeneration using embryonic stem cell-derived retinal pigment epithelium: preliminary results in Asian patients. Stem Cell Reports 4, 860–872. [PubMed: 25937371]

Staurenghi G, Sadda S, Chakravarthy U, Spaide RF, 2014. Proposed lexicon for anatomic landmarks in normal posterior segment spectral-domain optical coherence tomography: the IN*OCT Consensus. Ophthalmology 121, 1572–1578. [PubMed: 24755005]

Storm T, Burgoyne T, Dunaief JL, Christensen EI, Futter C, Nielsen R, 2019. Selective ablation of megalin in the retinal pigment epithelium results in megaophthalmos, macromelanosome

formation and severe retina degeneration. Invest. Ophthalmol. Vis. Sci 60, 322–330. [PubMed: 30665232]

Su N, Marz S, Plagemann T, Cao J, Schnittler HJ, Eter N, Heiduschka P, 2019. Occurrence of transmembrane protein 119 in the retina is not restricted to the microglia: an immunohistochemical study. Transl Vis Sci Technol 8, 29.

Sura AA, Chen L, Messinger JD, Swain TA, McGwin G Jr., Freund KB, Curcio CA, 2020. Measuring the contributions of basal laminar deposit and Bruch's membrane in age-related macular degeneration. Invest. Ophthalmol. Vis. Sci 61, 19.

Tan AC, Pilgrim M, Fearn S, Bertazzo S, Tsolaki E, Morrell A, Li M, Messinger JD, Dolz-Marco R, Nittala MG, Lei J, Sadda SR, Lengyel I, Freund KB, Curcio CA, 2018. Calcified nodules in retinal drusen are associated with disease progression with age-related macular degeneration. Sci. Transl. Med 10, 466–477.

Taubitz T, Fang Y, Biesemeier A, Julien-Schraermeyer S, Schraermeyer U, 2019. Age, lipofuscin and melanin oxidation affect fundus near-infrared autofluorescence. EBioMedicine 48, 592–604. [PubMed: 31648994]

Vogt SD, Curcio CA, Wang L, Li C-M, McGwin G Jr., Medeiros NE, Philp NJ, Kimble JA, Read RW, 2011. Retinal pigment epithelial expression of complement regulator CD46 is altered early in the course of geographic atrophy. Exp. Eye Res 93, 413–423. [PubMed: 21684273]

Warburton S, Davis WE, Southwick K, Xin H, Woolley AT, Burton GF, Thulin CD, 2007. Proteomic and phototoxic characterization of melanolipofuscin: correlation to disease and model for its origin. Mol. Vis 13, 318–329. [PubMed: 17392682]

Zanzottera EC, Ach T, Huisingh C, Messinger JD, Freund KB, Curcio CA, 2016. Visualizing retinal pigment epithelium phenotypes in the transition to atrophy in neovascular age-related macular degeneration. Retina 36 (Suppl. 1), S26–S39. [PubMed: 28005661]

Zanzottera EC, Messinger JD, Ach T, Smith RT, Curcio CA, 2015a. Subducted and Melanotic cells in advanced age-related macular degeneration are derived from retinal pigment epithelium. Invest. Ophthalmol. Vis. Sci 56, 3269–3278. [PubMed: 26024109]

Zanzottera EC, Messinger JD, Ach T, Smith RT, Freund KB, Curcio CA, 2015b. The Project MACULA retinal pigment epithelium grading system for histology and optical coherence tomography in age-related macular degeneration. Invest. Ophthalmol. Vis. Sci 56, 3253–3268. [PubMed: 25813989]

Zhang T, Kho AM, Srinivasan VJ, 2019. Improving visible light OCT of the human retina with rapid spectral shaping and axial tracking. Biomed. Opt Express 10, 2918–2931. [PubMed: 31259062]

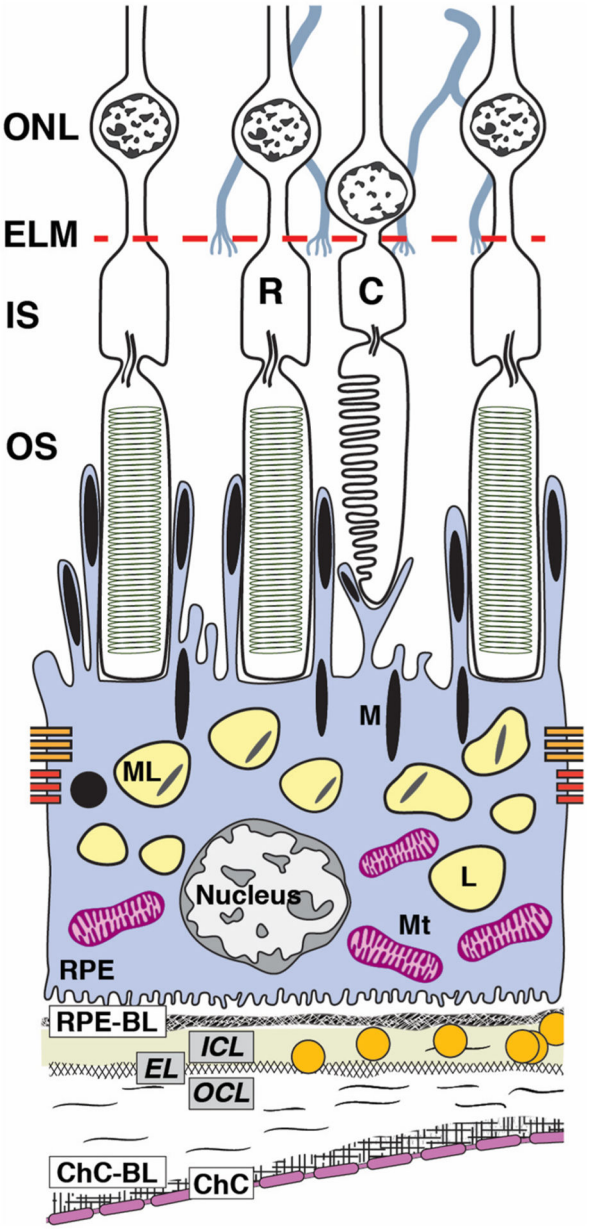

Fig. 1. Ultrastructure of retinal pigment epithelium (RPE) accessible in clinical imaging.

The RPE, as an epithelium, rests on a basal lamina (BL) of specialized extracellular matrix as it serves photoreceptors above and choroidal vasculature below. RPE cell bodies contaiñ1400 organelles of imaging significance in two cushions of similar numerosity (Bermond et al., 2020; Pollreisz et al., 2018, 2020): lipofuscin (L) and melanolipofuscin (ML) with some melanosomes(M) in the apical ¾, mitochondria (Mt) in the basolateral ¾, with the middle ½ containing both organelle classes. Apical processes are thin (0.3 µm in cross--section) and at least 15 µm long. Some surround rod outer segment tips at the cell body surface. Others extend upward to surround the shorter outer segment tips of cones. RPE-specific melanosomes are spindle-shaped (elongated), with ~2/3 in the apical processes and 1/3 at the apical aspect of the cell body, many standing upright.

Spherical non-autofluorescent electron-dense organelles may represent a second population of melanosomes. In consensus nomenclature for spectral domain OCT (Staurenghi et al., 2014), 4th reflective band components include RPE cell bodies, basal infoldings, RPE-BL, basal laminar deposit and/or contents of sub-RPE-BL space if present, and ICL-EL-OCL of BrM. The 3rd outer retinal hyperreflective band of OCT, called interdigitation zone (IZ), corresponds to interleaved outer segments and RPE apical processes with their organelles. For illustrative clarity, drawing and proportions of specific organelles are not to scale. C, cone; ChC, choriocapillaris; ChC-BL, ChC basal lamina; EL, Elastic layer; ELM, external limiting membrane; ICL, inner collagen layer; IS, inner segments of photoreceptor; M, melanosome; ML, melanolipofuscin; Mt, mitochondria; OCL, outer collagen layer; OS, outer segments of photoreceptors; R, rod; RPE, retinal pigment epithelium; RPE-BL, RPE basal lamina.

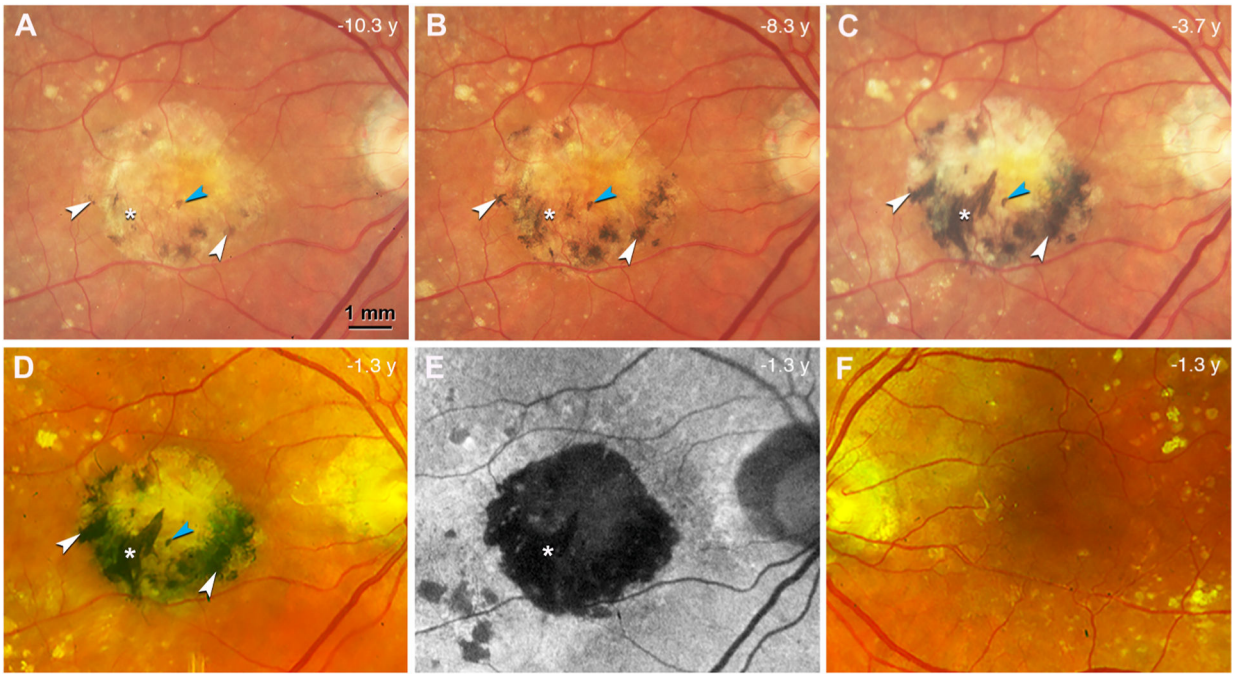

Fig. 2. Black pigment evolution in the index eye with neovascular age-related macular degeneration during 9 years of follow-up.

A-D. Color fundus photograph (CFP) of the right eye, acquired at different time points before patient death (in years) as indicated, shows a central subretinal fibrosis with increasing and darkening black pigment (white arrowheads). A prominent spear-like streak of black pigment developed over this time (white asterisk). One small spot of black pigment maintains stable during 9 years of follow up (blue arrowhead). Topcon camera, A-C; Optos California (Dunfermline Scotland), D. **E.** Fundus autofluorescence (FAF) at the last clinical visit, the same time point as in (D), shows that the fibrotic region is hypoFAF. The spear-like streak with black pigment is deeply hypoFAF (white asterisk). **F.** CFP of the left eye at the last clinical visit shows no black pigment or subretinal fibrosis.

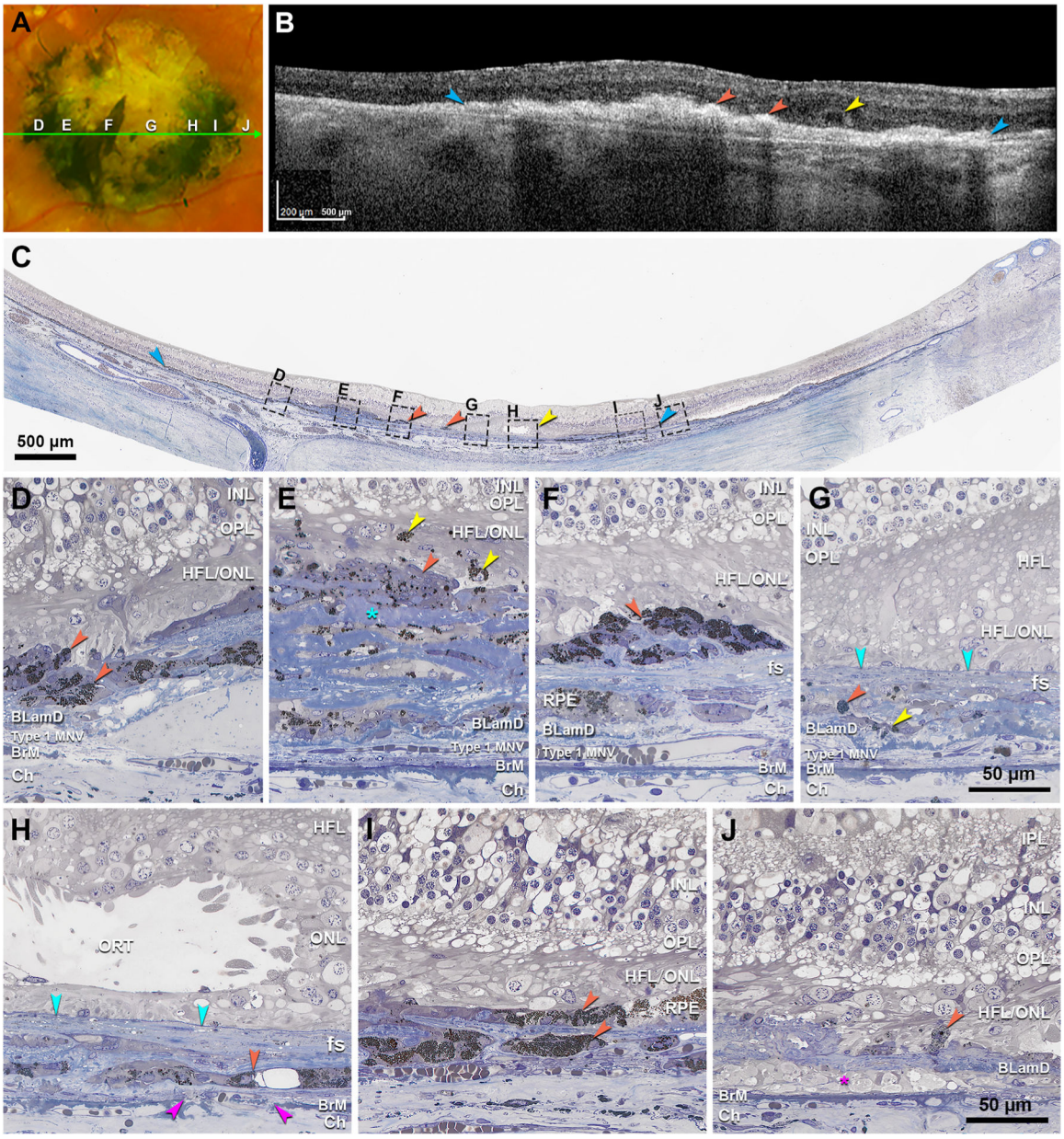

Fig. 3. Seven zones of distinct pigmentation examined by histology.

A. Color fundus photograph (CFP) of the right eye shows the central subretinal fibrotic area. Panels D–J show 7 zones with different pigmentation, as indicated. The green arrow line shows the location and direction of the OCT B-scan in panel B. **B.** OCT B-scan shows a large fibrotic scar (blue) with hyperreflective lesions (orange) and outer retinal tubulation (ORT, yellow). **C.** Panoramic view of histology shows fibrotic scar (blue), black cells (orange), and ORT (yellow) in correspondence with OCT (B), as well as 7 regions (D–J) corresponding with zones in (A) and magnified in (D–J). **D.** In a black pigmented area is a low mound of cells with moderately packed spherical melanosomes of uniform diameter (orange). **E.** In a gray pigmented area are cells with multiple nuclei and scattered dark spherical organelles (orange), mixed with reduplicated collagen stained in blue (teal

asterisk). These overlie basal laminar deposit (BLamD), which in turn covers type 1 macular neovascularization (MNV), recognized by endothelial tubes containing erythrocytes. Yellow arrowheads, singular and aggregated melanosomes within overlying neurosensory retina, with one at the right surrounding a small nucleus. **F.** In a black pigmented area are melanotic cells with dense dark spherical organelles, lying above the fibrotic scar (fs). **G.** In a pale-yellow zone, sparse melanosomes are found in two configurations: a granule aggregate within the scar (orange), and entombed retinal pigment epithelium (RPE, yellow) within the fs. A solid line delimits the MNV (teal). **H.** In a gray pigmented zone is a single layer of entombed RPE with spherical melanosomes, some large (orange). Fuchsia arrowheads indicate a Bruch's membrane (BrM) defect. **I.** In the black zone are two layers of melanotic cells with densely packed small spherical melanosomes of nearly uniform size (orange). **I.** A depigmented yellow zone corresponds to macular atrophy with persistent BLamD, sparse RPE granules (orange) and cellular processes in sub-RPE-basal laminar space (fuchsia asterisk). Green arrowhead, external limiting membrane (ELM) descent. Scale bar in F applies to C–F. Scale bar in I applies to G-I. BLamD, basal laminar deposit; BrM, Bruch's membrane; ChC, choriocapillaris; Ch, choroid; ELM, external limiting membrane; fs, fibrotic scar; HFL, Henle fiber layer; HFL/ONL, dyslamination of HFL and ONL; INL, inner nuclear layer; IPL, inner plexiform layer; IS, inner segments of photoreceptor; MNV, macular neovascularization; ONL, outer nuclear layer; OPL, outer plexiform layer; OS, outer segments of photoreceptor; PR, photoreceptor; RPE, retinal pigment epithelium.

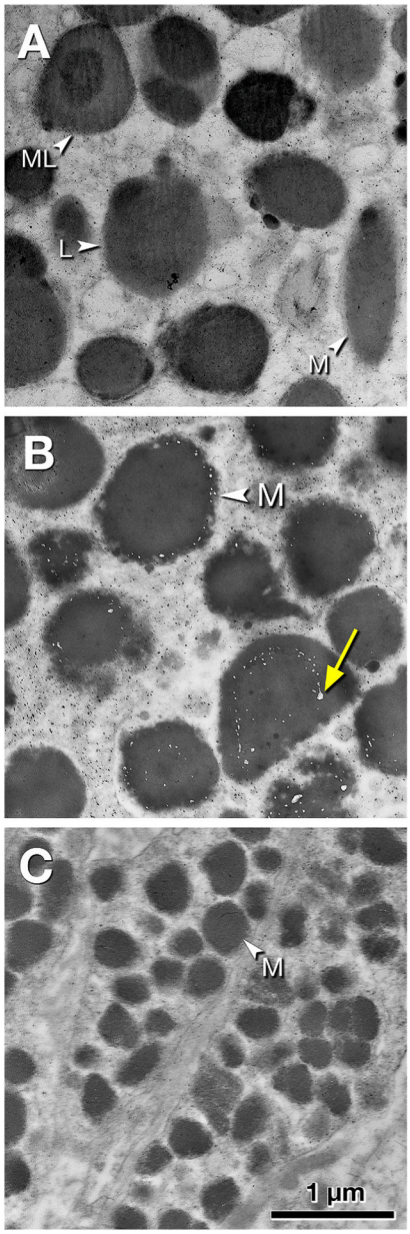

Fig. 4. Ultrastructure of melanosomes in outer retina and choroid of the index eye.

Retinal tissue is post-fixed with osmium-tannic acid-paraphenylenediamine. Scale bar in **C** applies to all panels. **A.** Organelles in phenotypic RPE cells outside the scar include spindle-shaped melanosomes (M), melanolipofuscin (ML) comprising an electron-dense interior and less dense exterior, and uniformly and moderately electron-dense lipofuscin (L). **B.** Melanosomes (M) in melanotic cells in the fibrotic scar are large, either spherical or ovoid, uniformly electron-dense, and covered with electron-lucent pits evenly spaced along the surfaces (yellow arrow). The latter have been considered mature melanosomes (Feeney, 1978). **C.** Melanosomes in choroidal melanocytes below the fibrotic scar are small, spherical or ovoid, and densely packed.

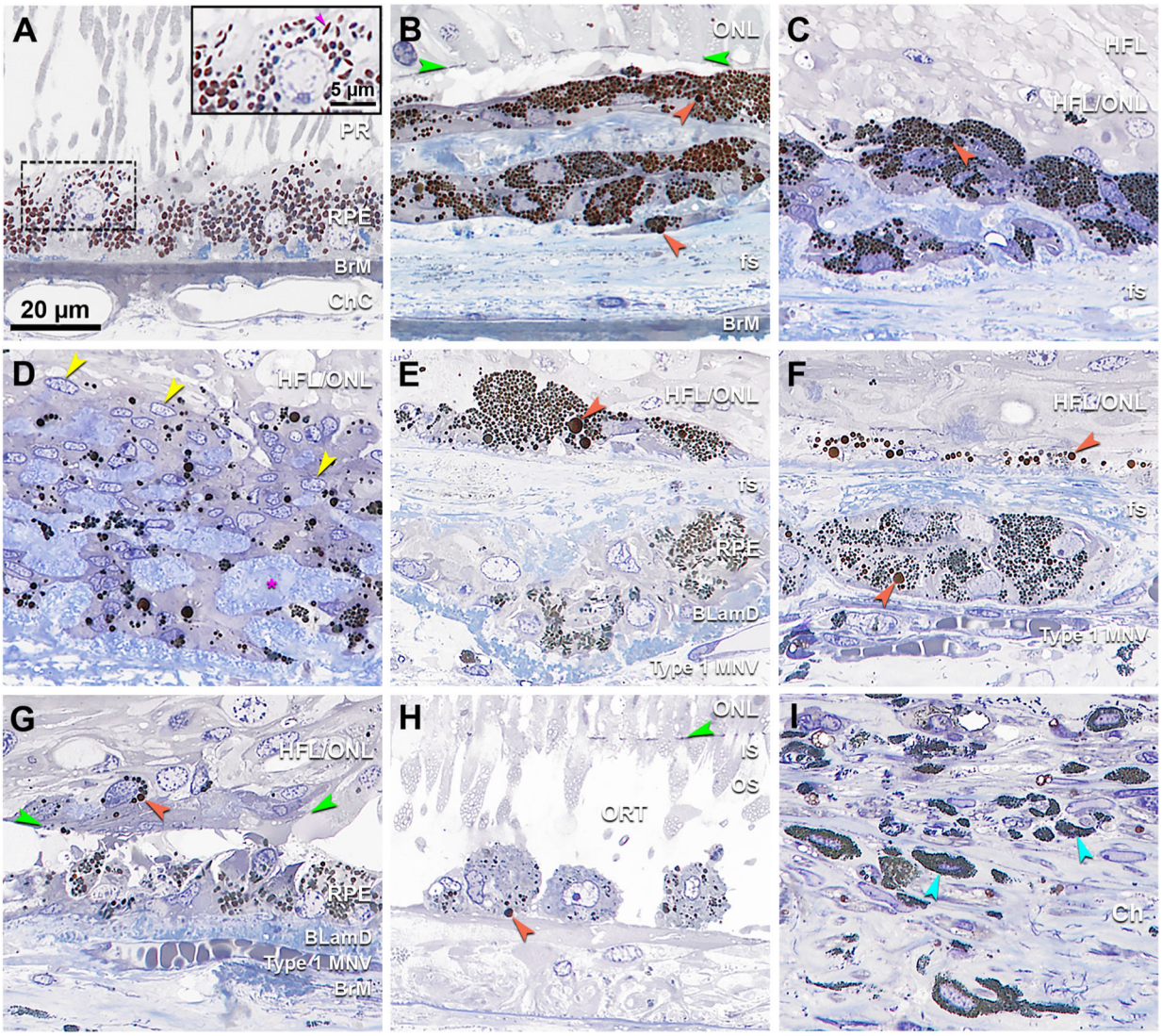

Fig. 5. Cells containing melanosomes in neovascular AMD, compared to age normal retinal pigment epithelium and choroidal melanocytes.

A. Age-normal retinal pigment epithelium (RPE) from the fellow eye has spindle shaped melanosomes at the apical aspect (inset, fuchsia arrowhead). Many granules of lipofuscin and melanolipofuscin are apparent elsewhere in this cell. **B.** Two layers of cells with densely packed dark spherical melanosomes, some large (orange). **C.** Cells with multiple nuclei and densely packed spherical melanosomes, some large (orange). **D.** Cells with multiple nuclei (yellow arrowheads) and scattered dark spherical melanosomes in different sizes mixed with collagen stained in blue (fuchsia asterisk). **E.** Cells with small spherical melanosomes mixed with several very large melanosomes (orange). An underlying layer of entombed RPE, adjacent to BLamD, contains many spindle-shaped melanosomes. **F.** Multinucleated cell with small spherical melanosomes with several very large melanosomes underneath the fs. A thin layer above the fs has dark spherical melanosomes in different sizes. **G.** A small cell body in the neurosensory retina, possibly microglial (Ma et al., 2013), is packed with spherical granules (orange). A layer of cells adjacent to BLamD contains both spherical

and spindle-shaped melanosomes. **H.** RPE-originated cells inside an open ORT (Schaal et al., 2015) showing sparse granules with one very large melanosome (orange). **I.** Relative to cells in panels B–H, choroidal melanocytes contain much smaller and more densely packed spherical melanosomes. Scale bar in A applies to all panels. BLamD, basal laminar deposit; BrM, Bruch's membrane; ChC, choriocapillaris; Ch, choroid; fs, fibrotic scar; HFL, Henle fiber layer; HFL/ONL, dyslamination of HFL and ONL; IS, inner segments of photoreceptor; MNV, macular neovascularization; ONL, Outer nuclear layer; OPL, outer plexiform layer; ORT, outer retinal tubulation; OS, outer segments of photoreceptor; PR, photoreceptor; RPE, retinal pigment epithelium.

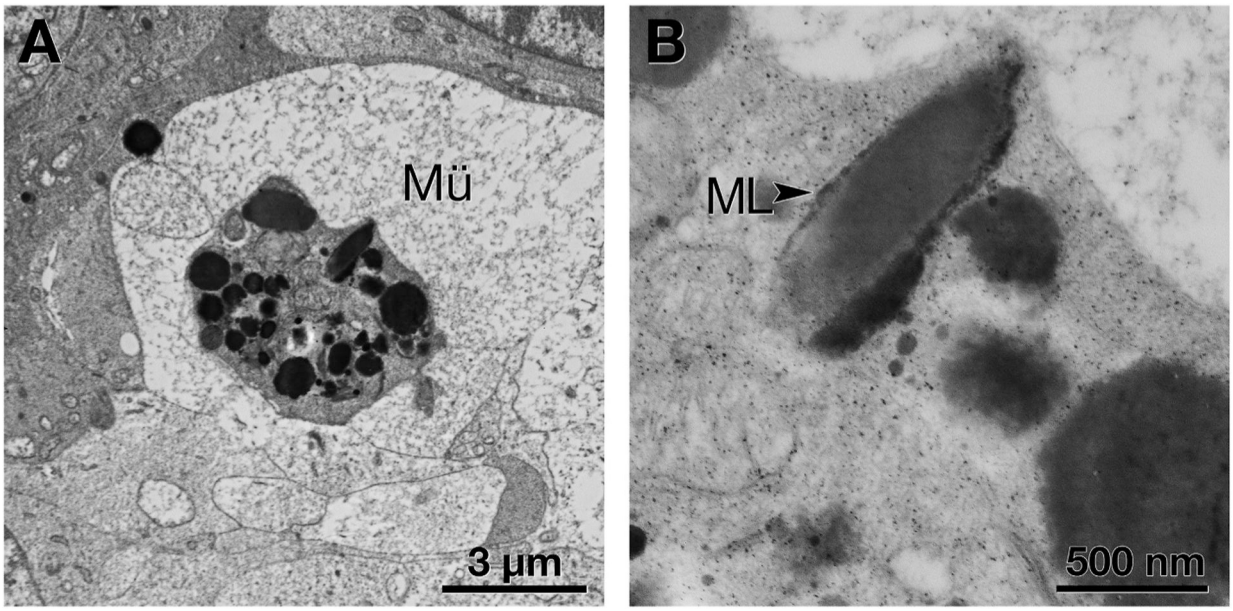

Fig. 6. Cellular fragment containing retinal pigment epithelium (RPE) organelles within Müller glia.

A. A Müller glial (Mü) process has enveloped an RPE cell fragment, recognized by its characteristic organelles. **B.** At higher magnification, an elongated organelle resembles that labeled melanolipofuscin (ML, black arrowhead) (Feeney, 1978).

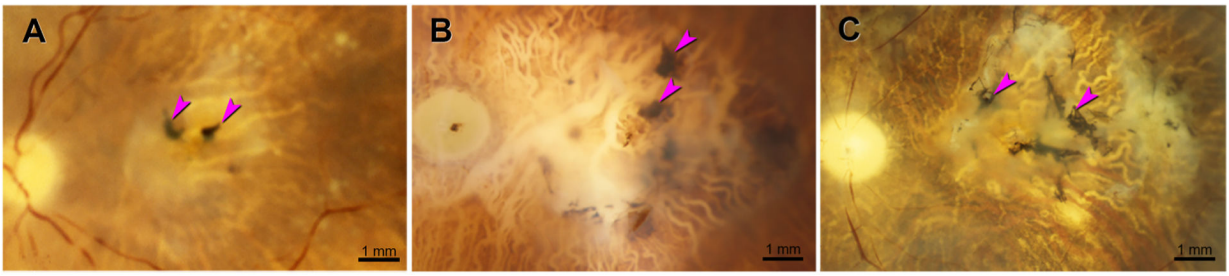

Fig. 7. Neovascular AMD eyes with black fundus pigment.

Ex vivo color photography, after removal of anterior segment. Fuchsia arrowheads indicate black pigment. Fibrotic scars are solid or translucent white. Underlying retinal pigment epithelium (RPE) is atrophic. Choroidal vessels emptied of blood are visible due to melanocytes between them. **A.** 93-year-old woman. **B.** 84-year-old man. RPE atrophy is extensive, and there is choroidal pallor near the optic nerve head. **C.** 86-year-old woman. Drusen are visible.

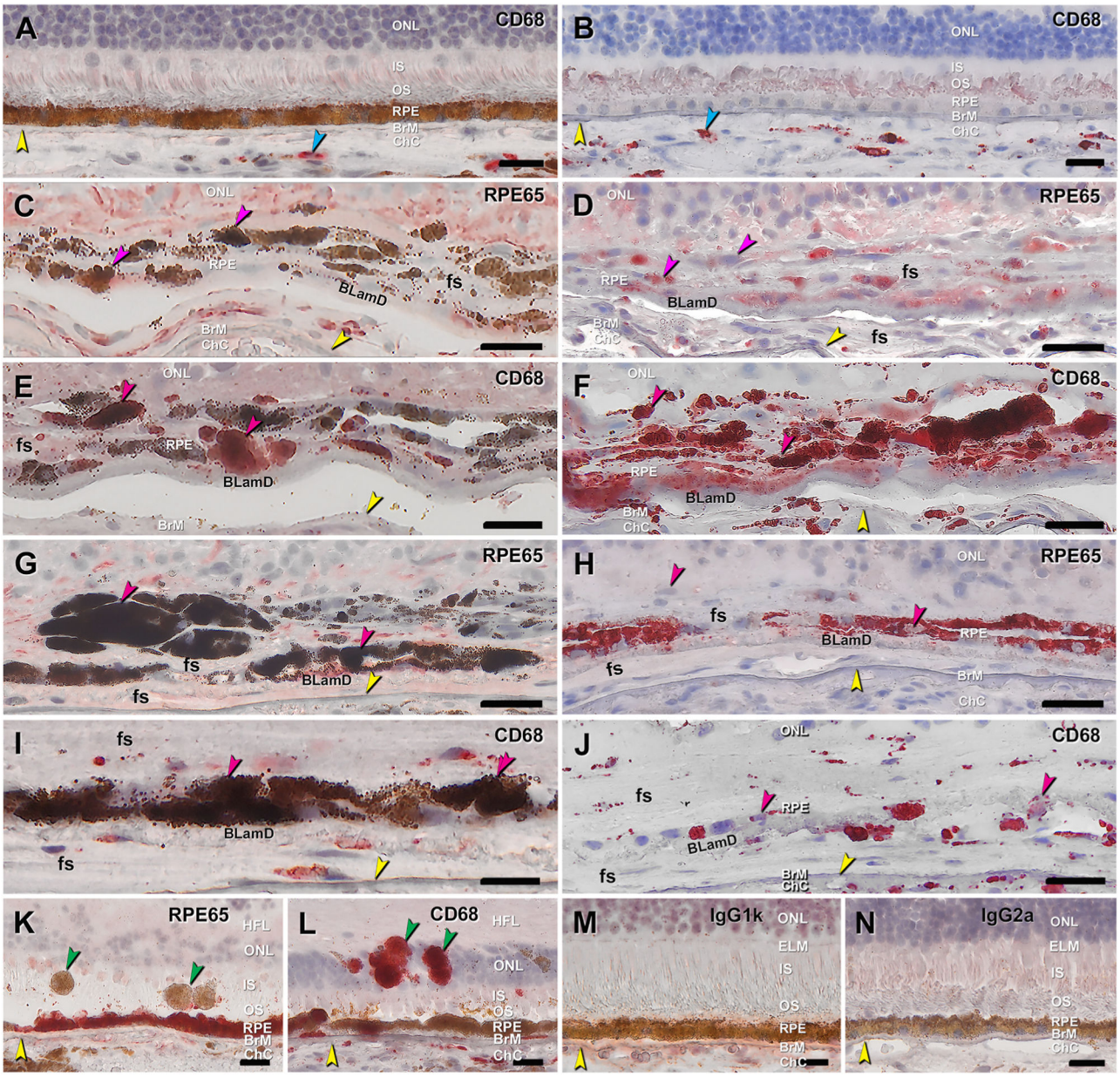

Fig. 8. Immunohistochemical localization of retinoid and immune markers in melanotic cells.

Twelve-μm-thick cryosections of human donor eyes were immunoprobed with antibodies RPE65 and CD68, in non-bleached (A, C, E, G, I) and bleached (B, D, F, H, J) neighboring sections from two donor eyes with neovascular age-related macular degeneration (first and second eye, C–F vs A, B, G-J, respectively). BrM is indicated by yellow arrowheads. All scale bars are 20 μm.

A-unbleached and **B-bleached** sections from same eye with G-J showed CD68 immunoreactivity in choroidal macrophages in both preparations (cyan arrowheads). **C-unbleached** and **D-bleached**. Variable RPE65 immunoreactivity is visible in melanotic cells with moderate levels of spherical melanosomes (pink arrowheads). **E-unbleached** and **F-bleached**. CD68 immunoreactivity is visible in melanotic cells with moderate levels of

spherical melanosomes (pink arrowheads). **G-unbleached** and **H-bleached.** Fewer fully pigmented melanotic cells exhibit RPE65 immunoreactivity (pink arrowhead) than the moderately pigmented cells (E, F). **I-unbleached** and **J-bleached.** Some fully pigmented melanotic cells are CD68 immunoreactive (pink arrowhead). **K.** Positive control: Normal RPE in RPE layer has strong RPE65 immunoreactivity whereas sloughed RPE in the bacillary layer lacks immunoreactivity (green arrowheads). **L.** Positive control: Normal RPE in RPE layer lacks CD68 immunoreactivity whereas intraretinal RPE is intensely immunoreactive (green arrowheads), as are choroidal macrophages and subducted RPE in the sub-RPE-basal lamina space (Zanzottera et al., 2015a). **M.** Negative control: Mouse IgG1k for RPE65. **N.** Negative control: Mouse IgG2a for CD68. BLamD, basal laminar deposit; BrM, Bruch's membrane; ChC, choriocapillaris; ELM, external limiting membrane; fs, fibrotic scar; HFL, Henle fiber layer; INL, inner nuclear layer; IS, inner segments of photoreceptor; OPL, outer plexiform layer; ONL, outer nuclear layer; OS, outer segments of photoreceptor; RPE, retinal pigment epithelium.

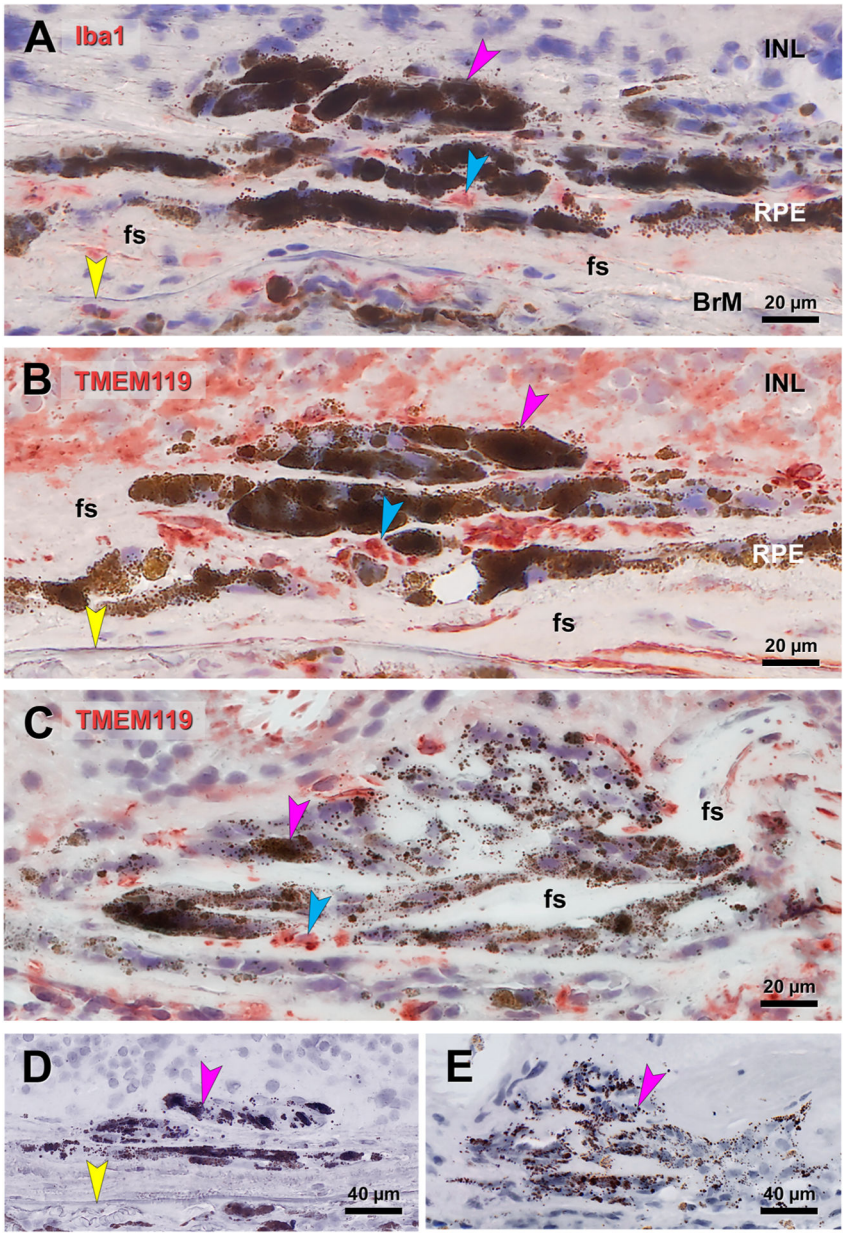

Fig. 9. Immunohistochemical localization of microglia and macrophages near melanotic cells.

Fuchsia arrowhead, cells containing large spherical melanosomes. Blue, red reaction product. Yellow arrowhead, Bruch's membrane. **A, B.** Immunoreactivity for Iba1 (A) and TMEM119 (B) localizes to fibrotic tissue between melanotic cells in the eye shown in Fig. 8GHIJ, as well as choroidal macrophages. Signal for TMEM119 is stronger overall and additionally localizes to overlying retina, in which ONL and HFL is completely degenerated. **C.** Immunoreactivity for TMEM119 localizes in areas between giant cells containing spherical melanosomes. **D, E.** Sham controls lacking primary antibody for Iba1 (D), in eye in A, and TMEM119 (E) in eye in C. BrM, Bruch's membrane; fs, fibrotic scar;

HFL, Henle fiber layer; INL, inner nuclear layer; ONL, outer nuclear layer; RPE, retinal pigment epithelium.